# Study on a set of bis-cyclometalated Ir(III) complexes with a common ancillary ligand†

**Younghun Byun,[a] Woo Sung Jeon,[a] Tae-Woo Lee,[a] Yi-Yeol Lyu,[a] Seok Chang,[a] Ohyun Kwon,*[a] Eunsil Han,[a] Heekyung Kim,[a] Myeongsuk Kim,[a] Ha-Jin Lee[b] and Rupasree Ragini Das*[a]**

***Received 12th December 2007, Accepted 12th May 2008***
***First published as an Advance Article on the web 15th July 2008***
**DOI: 10.1039/b719205c**



Bis-cyclometalated iridium(III) complexes [Ir($F_2$ppy)$_2$**ZN**] (**FZN**), [Ir($F_2$CNppy)$_2$**ZN**] (**FCZN**), [Ir(DMA$F_2$ppy)$_2$**ZN**] (**FDZN**) and [Ir(MeO$F_2$ppy)$_2$**ZN**] (**MeOFZN**) ($F_2$ppy = 4′,6′-difluoro-2-phenylpyridinate, $F_2$CNppy = 5′-cyano-4′,6′-difluoro-2-phenylpyridinate, DMA$F_2$ppy = 4′,6′-difluoro-4-dimethylamino-2-phenylpyridinate, MeO$F_2$ppy = 4′,6′-difluoro-4-methyl-2-phenylpyridinate and **ZN** = 3,5-dimethylpyrazole-*N*-carboxamide) emitting in the sky blue region were synthesized. We studied the effect of the ancillary ligand **ZN** and the substituents on the cyclometalating ligands on the crystal structures, photophysical and electrochemical properties and the frontier orbitals. Density functional theory (DFT) calculation results indicate that in **FCZN** and **FDZN** the cyclometalating ligands show negligible participation in the HOMO, the ancillary ligand **ZN** being the main participant along with the Ir(III) d-orbitals. **MeOFZN** exhibits the maximum photoluminescence quantum efficiency and radiative emission rates along with the dominant low frequency metal–ligand vibrations and maximum reorganization energy in the excited state. All the substituted complexes show more polar characteristics than **FZN**, **FCZN** possessing the highest dipole moment among the complexes. The performances of the solution-synthesised organic light emitting devices (OLEDs) of **FZN**, **FCZN** and **FDZN** doped in a blend of mCP (*m*-bis(*N*-carbazolylbenzene)) and polystyrene are studied.

## Introduction

The metal-to-ligand charge transfer (MLCT) excited states of transition metal complexes have been of great interest to explore the factors that determine and control the excited state photophysical and electrochemical properties for their applications as sensitizers in photochemical and photophysical processes,[1] biological labeling agents[2] and triplet emitters in organic light emitting devices (OLEDs).[3] The dynamics of the excited-state decay and its relation to the electronic effect of the various nonchromophoric and chromophoric ligands in a number of Os(II) and Ru(II) complexes have been investigated.[4] The studies demonstrate that the substituents at the chromophoric and nonchromophoric ligands influence redox potentials, absorption and emission energies, photoluminescence efficiencies and lifetimes.

The natures of the excited states of the Ir(III) complexes[5,6] in this line are extensively studied[7,8] and indicate that both the cyclometalating (analogous to the chromophoric ligands in ref. 4) and ancillary ligands (analogous to the nonchromophoric ligands in ref. 4) are important in influencing the electronic structures of the Ir(III) complex. Pyrazole derivatives have been studied as both the cyclometalating and the ancillary ligands in the Ir(III) complexes emitting in the blue region[2,7d,f–i,9,10] and have been found to influence the redox and photophysical properties to a greater extent when they are used as the cyclometalating ligands.[7f,g,i] Nonetheless, the ancillary ligands such as pyrazole-derivatized borates,[10] pyridyl pyrazolates[7g] also bring in systematic physical property changes. In this study we have coordinated a carboxamide-derivatized pyrazole (3,5-dimethylpyrazole-1-carboxamide) with Ir(III) in four bis-cyclometalated Ir(III) complexes as shown in Chart 1 and the crystal structures, frontier orbitals, photophysical and electrochemical properties of the complexes are investigated.

We examined a number of frontier molecular orbitals and the first eight singlet and eight triplet vertical transitions of these complexes using the DFT method. DFT calculations clearly show the participation of the 3,5-dimethylcarboxamide ligand in the charge transfer process, through the d-orbitals of the Ir(III) atom. Contrary to reports of the participation of the cyclometalating ligands in the highest occupied molecular orbital (HOMO),[7d,f,g,8,9a,10,11] the present study finds that, in **FCZN** and **FDZN**, the cyclometalating $F_2$CNppy (5′-cyano-4′,6′-difluoro-2-phenylpyridinate) and DMA$F_2$ppy (4′,6′-difluoro-4-dimethylamino-2-phenylpyridinate) ligands do not contribute to the HOMO. The room and low temperature emission spectra are interpreted to find out the metal participation in the MLCT nature of their electronic transition. The complexes were doped in

[a]*Samsung Advanced Institute of Technology, P. O. Box 111, Suwon, 440-600, Korea. E-mail: rd.rupasree@samsung.com, tigertom@dreamwiz.com*
[b]*Korea Basic Science Institute, Jeonju Center, Jeonju, 561-756, Korea*

† Electronic supplementary information (ESI) available: The associated frontier orbitals and energies obtained by DFT calculations on the complexes, calculated vertical transitions and atomic charges from Mulliken population analysis of the complexes, experimental methods. CCDC reference numbers 670853–670855. For ESI and crystallographic data in CIF or other electronic format see DOI: 10.1039/b719205c

 

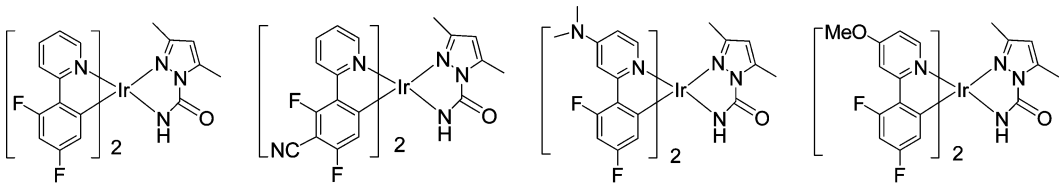

**FZN** **FCZN** **FDZN** **MeOFZN**

**Chart 1**

the host mCP (*m*-bis(*N*-carbazolylbenzene))[12] in the polystyrene blend and the electroluminescence properties were studied.

## Results and discussion

### Synthesis

The starting materials, $[Ir(F_2ppy)_2Cl]_2$, $[Ir(F_2CNppy)_2Cl]_2$, $[Ir(DMAF_2ppy)_2Cl]_2$ and $[Ir(MeOF_2ppy)_2Cl]_2$ ($F_2ppy$ = 4′,6′-difluoro-2-phenylpyridinate, $MeOF_2ppy$ = 4′,6′-difluoro-4-methyl-2-phenylpyridinate) were synthesized from $IrCl_3{\cdot}3H_2O$ (Acros Chemicals), and the cyclometalating ligands based on the literature procedure.[13] The deprotonation of the ancillary ligand was indeed achieved at room temperature without the aid of any base. The synthetic procedure of the **FZN**, **FCZN**, **FDZN** and **MeOFZN** complexes are given in the ESI.†

### Crystal structure and DFT calculations

Single-crystals of the complexes were grown by the slow layer diffusion of diethyl ether or hexane into the methylene chloride solution. Since most crystals lose their structural solvents of crystallization within a few minutes of exposure to air, they were coated with oil, and the intensity data were collected with Mo $K_\alpha$ radiation ($\lambda$ = 0.71073 Å) on a Bruker SMART CCD equipped with a graphite crystal, incident-beam monochromator. All crystallographic data were corrected for the Lorentz and polarization effects, and semi-empirical absorption corrections based on equivalent reflections were applied. The crystal structures were solved by direct methods and refined by full-matrix least-squares calculations with the SHELXTL-PLUS program package (Ver. 5.1). All the non-hydrogen atoms were refined anisotropically, and hydrogen atoms were added to their geometrically ideal positions. The disordered solvent molecule was treated using the SQUEEZE program in the case of **FCZN** for better structure refinement. The ORTEP diagrams and crystal packing of the neighboring molecules of the **FZN** and **FCZN** complexes are presented in Fig. 1 and the crystallographic and structure refinement in Table 1.

DFT calculations have been carried out to find the global minimum geometry and excitation energies by using the B3LYP functional with the LANL2DZ basis set for the Ir atom and 6-31G(d) basis set for the ligand atoms.[14] All calculations were performed by Gaussian 98 program.[15] The overall calculated geometrical parameters are in quite good agreement with those of crystal structures (Table 2). In the complexes, the Ir(III) center is octahedrally coordinated to two cyclometalating ligands and the ancillary ligand 3,5-dimethylpyrazole-*N*-carboxamide. In the complexes the Ir–$N_1$ bond length is longer than that of Ir–$N_3$,

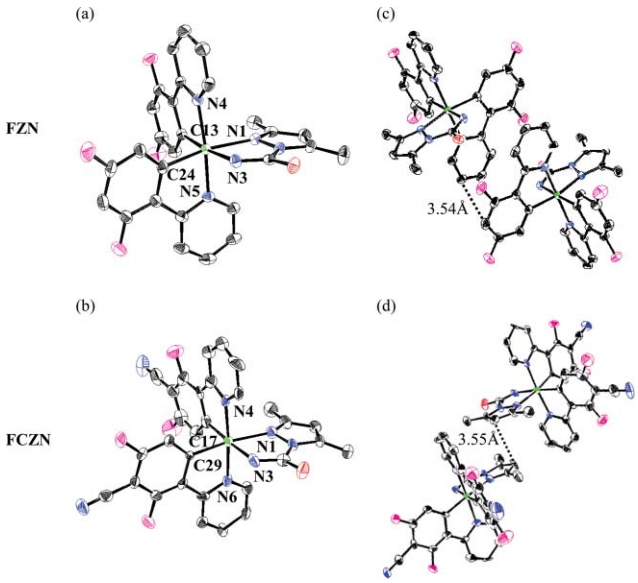


**Fig. 1** ORTEP diagrams of the complexes with 50% probability with atom labeling (hydrogen atoms are omitted for clarity): (a) **FZN**; (b) **FCZN**. Closest molecules showing packing effects, the dotted lines indicate the weak intermolecular non-bonding contacts: (c) **FZN**; (d) **FCZN**.

implying a stronger bond formation between the metal center and the carboxamide group than the pyrazole nitrogen. The crystal packing of the **FZN** complex exhibits π–π interactions[16] between the neighboring molecules as has been observed by the distance of 4.13 Å between the aromatic planes in the **FZN** complex.

The highest occupied molecular orbitals (HOMOs) and the lowest unoccupied molecular orbitals (LUMOs) of **FZN**, **FCZN**, **MeOFZN** and **FDZN** from DFT calculations are shown in Fig. 2. In **FZN**, the HOMO represents a mixture of the d-orbitals of the Ir(III) atom, phenyl rings of both the cyclometalating ligands and the carboxamide portion of the 3,5-dimethylpyrazole carboxamide[7d,f,g,8,9a,11] while the LUMO is predominantly the cyclometalating ligand in character and spreads entirely over the two $F_2ppy$ ligands. Both the HOMO and the LUMO demonstrate π-symmetry. In **FZN**, $S_1$ (404 nm) and $S_2$ (396 nm) transitions (see ESI†) have low oscillator strengths and correspond to the absorption features around 418–440 nm with the extinction coefficients of 260–500 $mol^{-1}$ $cm^{-1}$. These transitions are suggested to have less singlet character and could be mixed with the triplet transitions of $T_3$ and $T_4$ at the calculated values of 405 and 401 nm, respectively. The broad band in the 385–370 nm in the absorption spectra of **FZN** is ascribed to the transitions $S_3$ and $S_4$. The calculated $T_1$ and $T_2$ at 446 and 438 nm agree well with the experimental absorption peaks at 455 and 428 nm, respectively.

**Table 1** Crystallographic data and structure refinement of **FZN** and **FCZN**

| | **FZN** | **FCZN** |
|---|---|---|
| Empirical formula | $C_{28}H_{20}F_4IrN_5O$ | $C_{30}H_{18}F_4IrN_7O$ |
| Formula weight | 710.69 | 760.71 |
| Temperature/K | 293(2) | 293(2) |
| Wavelength/Å | 0.71073 | 0.71073 |
| Crystal system | Monoclinic | Monoclinic |
| Space group | $P2_1/n$ | $C2/c$ |
| Unit cell dimensions: | | |
| $a$/Å | 11.572(2) | 21.982(11) |
| $b$/Å | 9.523(2) | 30.270(15) |
| $c$Å | 22.409(5) | 14.317(7) |
| $\alpha$/° | 90 | 90 |
| $\beta$/° | 96.012(4) | 127.848(7) |
| $\gamma$/° | 90 | 90 |
| Volume/Å$^3$ | 2455.9(9) | 7523(7) |
| $Z$ | 4 | 8 |
| Density (calculated)/Mg m$^{-3}$ | 1.922 | 1.343 |
| Absorption coefficient/mm$^{-1}$ | 5.500 | 3.598 |
| $F$(000) | 1376 | 2944 |
| Crystal size/mm | 0.38 × 0.25 × 0.15 | 0.25 × 0.15 × 0.03 |
| Theta range for data collection/° | 1.83 to 28.28 | 1.35 to 25.00 |
| Indices | $-14 \le h \le 15$<br>$-12 \le k \le 11$<br>$-28 \le l \le 29$ | $-25 \le h \le 26$<br>$-35 \le k \le 35$<br>$-16 \le l \le 17$ |
| Reflections collected | 14916 | 17507 |
| Independent reflections [$R$(int)] | 5851 [0.0215] | 6487 [0.0855] |
| Completeness to theta | 28.28°, 96.0% | 25.00°, 97.7% |
| Absorption correction | Semi-empirical from equivalents | None |
| Max. and min. transmission | 0.4925 and 0.2290 | 0.8997 and 0.4666 |
| Refinement method | Full-matrix least-squares on $F^2$ | Full-matrix least-squares on $F^2$ |
| Data/restraints/parameters | 5851/0/354 | 6487/0/390 |
| Goodness-of-fit on $F^2$ | 1.054 | 1.087 |
| Final R indices [$I > 2\sigma(I)$] | $R1 = 0.0225$, $wR2 = 0.0499$ | $R1 = 0.0883$, $wR2 = 0.2241$ |
| $R$ indices (all data) | $R1 = 0.0280$, $wR2 = 0.0517$ | $R1 = 0.1294$, $wR2 = 0.2401$ |
| Largest diff. peak and hole/e Å$^{-3}$ | 1.561 and −0.757 | 2.223 and −3.387 |

**Table 2** Selected bond length and angles from the experimental and theoretical results

| Bond distance/Å | | | Bond angle/° | | |
|---|---|---|---|---|---|
| | Calc. | Exptl | | Calc. | Exptl |
| **FZN** | | | | | |
| Ir–$N_4$ | 2.074 | 2.048(2) | $C_{13}$–Ir–$C_{24}$ | 89.5 | 90.56(11) |
| Ir–$C_{13}$ | 2.030 | 2.016(3) | $C_{13}$–Ir–$N_1$ | 100.6 | 100.73(10) |
| Ir–$N_5$ | 2.068 | 2.039(2) | $C_{24}$–Ir–$N_3$ | 96.0 | 93.84(11) |
| Ir–$C_{24}$ | 2.011 | 2.005(3) | $C_{13}$–Ir–$N_3$ | 172.9 | 173.68(10) |
| Ir–$N_1$ | 2.223 | 2.142(2) | $N_1$–Ir–$N_3$ | 74.2 | 75.38(9) |
| Ir–$N_3$ | 2.154 | 2.104(2) | $C_{13}$–Ir–$N_4$ | 80.0 | 80.25(11) |
| | | | $C_{13}$–Ir–$N_5$ | 96.8 | 94.24(10) |
| | | | $C_{24}$–Ir–$N_4$ | 96.1 | 95.91(11) |
| | | | $C_{24}$–Ir–$N_5$ | 80.3 | 80.43(11) |
| **FCZN** | | | | | |
| Ir–$N_4$ | 2.075 | 2.050(13) | $C_{17}$–Ir–$C_{29}$ | 89.4 | 85.0(6) |
| Ir–$C_{17}$ | 2.027 | 1.979(16) | $C_{17}$–Ir–$N_1$ | 100.5 | 102.6(6) |
| Ir–$N_6$ | 2.070 | 2.060(13) | $C_{29}$–Ir–$N_3$ | 96.0 | 96.2(5) |
| Ir–$C_{29}$ | 2.008 | 1.986(14) | $C_{29}$–Ir–$N_1$ | 101.2 | 171.4(5) |
| Ir–$N_1$ | 2.214 | 2.148(12) | $N_1$–Ir–$N_3$ | 74.4 | 76.5(5) |
| Ir–$N_3$ | 2.149 | 2.071(14) | $C_{17}$–Ir–$N_4$ | 80.1 | 79.3(6) |
| | | | $C_{17}$–Ir–$N_6$ | 96.9 | 96.4(6) |
| | | | $C_{29}$—Ir–$N_4$ | 96.3 | 95.8(5) |
| | | | $C_{29}$–Ir–$N_6$ | 80.4 | 80.6(5) |

Calculated $T_5$ transition at 383 nm coincides with $S_3$ transition and also has the same orbital parentage (H − 1 → L). Since this transition corresponds to the onset of the absorption band at 390–370 nm region, and has significant molar extinction coefficient of 1300 mol$^{-1}$ cm$^{-1}$, it can have the attributes of strongly mixed singlet and triplet MLCT character. The $T_6$ transition at 378 nm has contributions from the processes (H − 3 → L + 1) and (H → L + 1), where H − 3 is centered on the cyclometalating ligand and the HOMO is contributed to by the ligands and Ir(III) d-orbitals, and L + 1 is a purely ligand centered orbital; it clearly indicates that the band in the 390–370 nm region includes a pure cyclometalating ligand based π–π* transition along with the singlet and triplet MLCT transitions.

**MeOFZN** shows similar orbital contributions to the HOMO as **FZN**, whereas in **FCZN** and **FDZN** we notice almost negligible participation of the cyclometalating ligands in the HOMO. The Ir(III) d-orbitals and carboxamide group of the **ZN** ligand only participate in HOMO. Such differences in the orbital parentage of the HOMO of **FCZN** and **FDZN** from **FZN** and **MeOFZN** indicate the strong impact of the substituents on the orbitals participating in the electronic transitions. The absorption spectra of the complexes are in good agreement with the calculated transitions. The calculated dipole moments of the complexes **FZN**, **FCZN**, **MeOFZN** and **FDZN** are 3.39, 9.68, 4.38 and 3.0 D, respectively. The **FCZN** complex has the highest dipole moment value which is ascribed to the high electron withdrawing nature of the cyano group. A similar increase of the dipole moment is observed in the *fac*-Ir(5-Phppy)$_3$ (7.49 D) compared to the

 

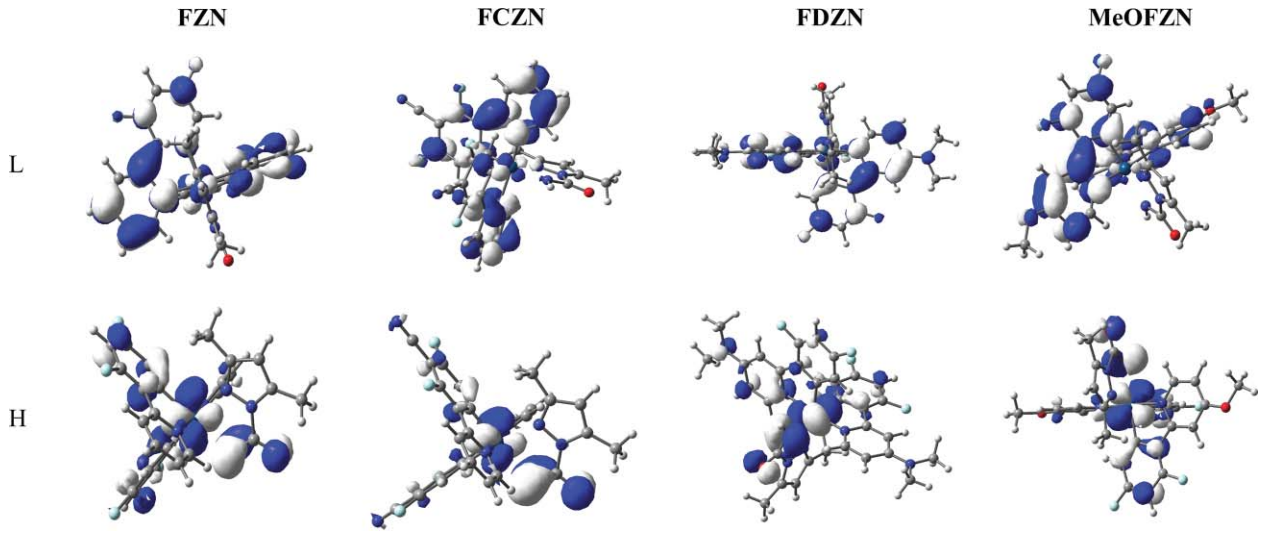


**Fig. 2** HOMO and LUMO of **FZN**, **FCZN**, **FDZN** and **MeOFZN**. Assignments: H = HOMO, L = LUMO.

*fac*-Ir(ppy)$_3$ (6.53 D), when the electron withdrawing phenyl group is substituted at the 5-position of the phenyl ring (5-Phppy = 2-(5-phenyl)phenylpyridinate, ppy = 2-phenylpyridinate).[17]

### Electrochemical properties

The electrochemical redox potentials (Table 3) were monitored by cyclic voltammetry and square wave voltammetry (SWV).[18] The cyclic voltammograms of these complexes show quasi-reversible oxidation processes (see ESI†). The $i_{pa}/i_{pc}$ values of **FZN**, **FCZN**, **MeOFZN**, and **FDZN** under the 100 mV s$^{-1}$ scan were 0.7, 0.5, 0.8 and 0.9, respectively.[19] The $E_{1/2}$(oxd) values of the complexes **FZN**, **FCZN**, **MeOFZN**, and **FDZN** were determined using SWV (Fig. 3a) relative to a ferrocene/ferrocenium redox potential and found to be 0.77, 1.04, 0.67 and 0.48 V, respectively.

The oxidation potentials follow the increasing order of **FCZN** > **FZN** > **MeOFZN** > **FDZN**. This can be attributed to the more electron-withdrawing effect of the CN group in the phenyl ring decreasing the electron density at the *ortho*-metalating carbon atom and consequently the Ir(III) center. Thus the HOMO electrons in **FCZN** become hard to remove compared to **FZN**. On the other hand, the electron donating methoxy and dimethylamino groups increase the electron densities of the pyridyl rings of **MeOFZN** and **FDZN**; this increases the electron density at the metal center upon coordination. It becomes easier to remove the electron from the HOMO of **MeOFZN** and **FDZN** than **FZN**. The higher anodic shift of the oxidation potential of **FDZN** compared to **MeOFZN** can be attributed to the more electron donating effect of the dimethylamino group than the methoxy group. A valid point may arise at this instant: how would the HOMO of **FDZN** and **FCZN** be affected by the substituents in the respective cyclometalating ligands, when these ligands do not contribute to the HOMO as found by the DFT calculations? However, the DFT calculations show that the H − 1 orbitals in these two complexes

**Table 3** Thermal, photophysical and electrochemical properties of the complexes

| | **FZN** | **FCZN** | **FDZN** | **MeOFZN** |
|---|---|---|---|---|
| $A$/nm ($\varepsilon$/dm$^3$ mol$^{-1}$ cm$^{-1}$)[a] | 293(12 174), 329(5428), 360(3798), 380(3316), 428(932), 456(356) | 292(15 834), 328(6263), 356(3618) 378(2562), 417(524), 446(334) | 290(13 937), 317(9354), 345(7324), 375(4679), 438(593) | 291(8514), 320(4813), 356(3798), 377(2870), 451(222) |
| $^1$MLCT[a]/eV | 3.26 (380 nm) | 3.28 (378 nm) | 3.30 (375 nm) | 3.29 (377 nm) |
| PL$_{soln}$[a]/nm | 484 | 485 | 475 | 477 |
| PL$_{soln}$[b]/nm | 474 | 465 | 474 | 469 |
| PL$_{PMMA\ film}$[f]/nm | 474 | 467, 483 | 479 | 470, 485 |
| $\tau_{PMMA\ film}$/μs | 1.20 | 1.50 | 1.18 | 1.28 |
| $\phi_{PL}$ (%) | 21 | 40 | 28 | 70 |
| $K_r \times 10^{-5}$ | 1.75 | 2.66 | 2.37 | 5.46 |
| $K_{nr} \times 10^{-5}$ | 6.58 | 4.00 | 8.47 | 2.34 |
| $E_{1/2}$(oxd)[c]/V | 0.77 | 1.04 | 0.48 | 0.65 |
| HOMO[d]/eV | 6.07 | 6.34 | 5.78 | 5.95 |
| $E_{1/2}$(red)[c]/V | −2.55 | −2.32 | −2.87 | −2.75 |
| LUMO[d]/eV | 2.75 | 2.98 | 2.43 | 2.55 |
| LUMO[e]/eV | 2.81 | 3.06 | 2.48 | 2.63 |
| $\Delta E_{1/2}$[c]/eV | 3.32 (363 nm) | 3.36 (369 nm) | 3.35 (370 nm) | 3.40 (364 nm) |

[a] Obtained from 2-Me-THF solution. PL = photoluminescence. [b] Obtained from methylene chloride solution. [c] Measured by square wave voltammetry (SWV) method. [d] Calculated from electrochemical experimental values. [e] Calculated from the HOMO obtained from the electrochemical experimental values and $^1$MLCT absorption energies. [f] PMMA = polymethylmethacrylate.

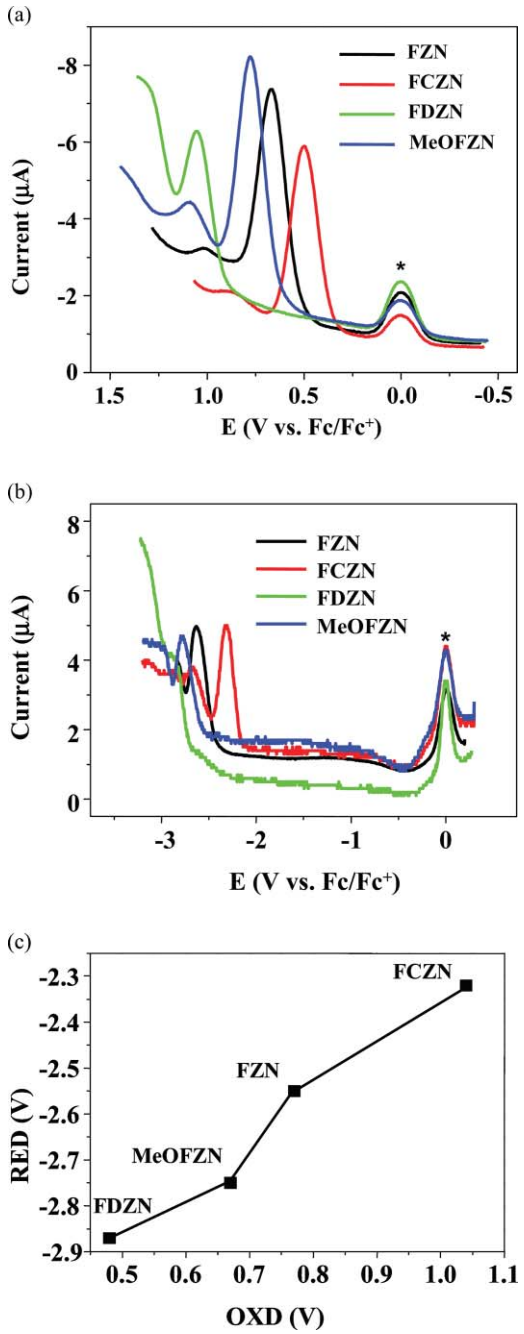


**Fig. 3** (a) Square wave voltammograms of the complexes in the oxidation region. (b) Square wave voltammograms of the complexes in the reduction region. Ferrocenium/ferrocene reduction peak is marked with asterisk. (c) Comparative plot of oxidation and reduction potentials.

have contributions from the cyclometalating ligands, there being a difference of 0.1 eV between HOMO and H − 1. This implies that the H and H − 1 can be mixed depending upon which of the cyclometalating ligands can influence the HOMO energies. We have also observed a similar anodic shift of the oxidation potential in a dimethyl-substituted cyclometalated Ir(III) complex compared to an unsubstituted complex.[8]

The differential pulsed reduction voltammograms of the complexes are shown in Fig. 3b. The first reduction potentials of **FZN**, **FCZN**, **MeOFZN**, and **FDZN** were observed at −2.55, −2.32, −2.75 and −2.87 V, respectively.[20] The second reduction processes were detected at −3.04, −2.65 and −3.10 V for **FZN**, **FCZN**, and **MeOFZN**, respectively. The second reduction peak of **FDZN** could not be obtained in the limit of the potential window of the experimental conditions. The two reduction processes take place at the two cyclometalated ligands consistent with related cyclometalated Ir(III) complexes.[21,22] The cathodic shifts in the reduction potentials follow the sequence of **FCZN** < **FZN** < **MeOFZN** < **FDZN**, which is the reverse order of the anodic shifts of the oxidation potentials of the complexes. Since the oxidation and reduction potentials are related to the HOMO and LUMO levels, it is evident that both the HOMO and the LUMO are raised in energy in the order **FDZN** > **MeOFZN** > **FZN** > **FCZN**. Interestingly, even if the substituents with very strong inductive effects are incorporated in the cyclometalating ligands, the electrochemical gaps of these complexes remain almost the same (3.32–3.41 V) and are consistent with the similar $^1$MLCT absorption peaks around 375–380 nm in their absorption spectra. Both the reduction potentials (−2.32 to −2.87 V) and oxidation potentials (0.48 to 1.04 V) demonstrate similar ranges conclusive of the fact that both the HOMO and LUMO of these complexes are equally affected by the substituents on the cyclometalating ligands. Fig. 3c shows the parallel variations in the $E_{1/2}$(red) and $E_{1/2}$(oxd) values.

## Photophysical properties

The absorption and emission spectra of the complexes are summarized in Table 3 and shown in Fig. 4. The bands below 300 nm correspond to the π–π* transitions of aromatic ligands,[4b,21,23] as evidenced by their high extinction coefficients of the order $10^5$ dm$^3$ mol$^{-1}$ cm$^{-1}$. The spectral region of 385 to 325 nm demonstrates three clear bands ($\varepsilon$ = 6400–1600 dm$^3$ mol$^{-1}$ cm$^{-1}$) in all of the cases. These bands can be attributed to the admixture of the metal-to-ligand charge transfer and ligand based π–π* transitions. The bands around 375 nm can be ascribed to the $^1$MLCT transitions ($\varepsilon$ = 4580–2760 dm$^3$ mol$^{-1}$ cm$^{-1}$).[4] The lowest energy absorption bands at 456 nm ($\varepsilon$ = 356 dm$^3$ mol$^{-1}$ cm$^{-1}$) and 446 nm ($\varepsilon$ = 334 dm$^3$ mol$^{-1}$ cm$^{-1}$), with diminished intensities in the absorption spectra of **FZN** and **FCZN**, are assigned as forbidden triplet ($T_1$) transitions.[24,25,26] Similar features are reported for the complexes using tetrapyrazolylborate.[7d] **FDZN** and **MeOFZN** do not demonstrate sharp absorption features in the longer wavelength region (Fig. 5b), instead broad bands are observed around 438 nm ($\varepsilon$ = 593 dm$^3$ mol$^{-1}$ cm$^{-1}$) and 451 nm ($\varepsilon$ = 222 dm$^3$ mol$^{-1}$ cm$^{-1}$) in **FDZN** and **MeOFZN**, respectively.

The $^1$MLCT absorption peaks at 380 nm (3.26 eV) ($\varepsilon$ = 3316 dm$^3$ mol$^{-1}$ cm$^{-1}$), 378 nm (3.28 eV) ($\varepsilon$ = 2562 dm$^3$ mol$^{-1}$ cm$^{-1}$), 375 nm (3.30 eV) ($\varepsilon$ = 4679 dm$^3$ mol$^{-1}$ cm$^{-1}$) and 377 nm (3.29 eV) ($\varepsilon$ = 2870 dm$^3$ mol$^{-1}$ cm$^{-1}$) for **FZN**, **FCZN**, **FDZN**, and **MeOFZN** are in good agreement with their observed electrochemical gaps ($\Delta E_{1/2}$) of 3.32, 3.36, 3.35 and 3.40 eV, respectively. The difference between the $\Delta E_{1/2}$ and $^1$MLCT energies of **FZN**, **FCZN**, **FDZN**, and **MeOFZN** are 0.06, 0.08, 0.05 and 0.10 eV, respectively. **MeOFZN** shows the highest difference between the $\Delta E_{1/2}$ and $^1$MLCT values indicating that the reorganization energy upon excitation is highest in this complex implying less metal participation in the charge transfer state compared to the other complexes.

 

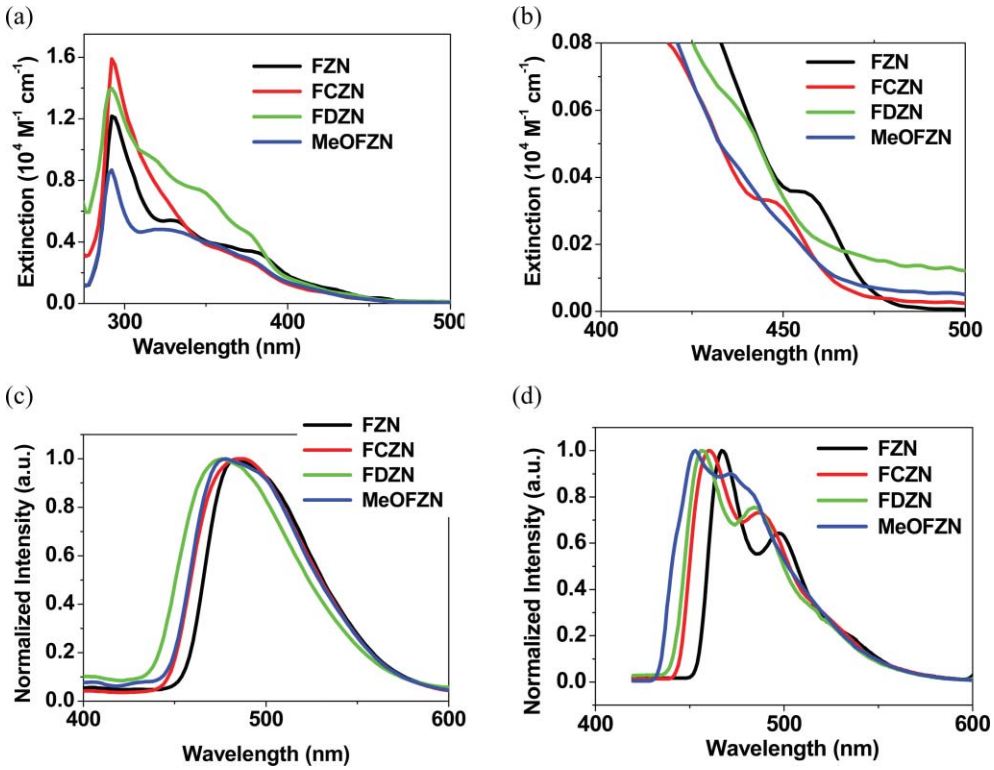


**Fig. 4** (a) Absorption spectra, (b) absorption spectra in the $^3$MLCT region, (c) emission spectra at room temperature, and (d) emission spectra of the complexes at 77 K in 2-Me-THF.

All of these complexes are highly emissive both in the solution and solid state at room temperature and demonstrate single emission peaks in the range of 485–475 nm in 2-Me-THF solution (Fig. 4c). The peak emissions are blue shifted in methylene chloride solution and PMMA doped films indicating a solvatochromic effect in these complexes. Broadening of the emission spectra toward the blue region is observed in the substituted complexes. The full width at half maximum (FWHM) of the PL spectra of **FZN**, **FCZN**, **FDZN**, and **MeOFZN** are 2556, 2847, 2823 and 2979 $cm^{-1}$, respectively, indicating that the substitutions increase the vibrational distortions and higher reorganizational energies of the excited state. However, the peak emission energies are almost the same (2.56–2.61 eV) in all of these complexes (Table 3), contrary to the emissions observed from the corresponding picolinate derivatives Ir($DMF_2$ppy)$_2$(pic) (550 nm, 2.25 eV), Ir($F_2$ppy)$_2$(pic) (470 nm, 2.63 eV) and Ir($F_2$CNppy)$_2$(pic) (452 nm, 2.74 eV).[27] This indicates that in a similar series of cyclometalating ligands the photophysical properties of the iridium complexes may not follow the same sequence when the ancillary ligand is changed.

The emission spectra at 77 K (Fig. 4d, Table 4) demonstrate vibrational progressions in all the complexes. The peak emissions ($E_{em}$(0–0)) are blue shifted by 17, 25, 19 and 25 nm for **FZN**, **FCZN**, **FDZN**, and **MeOFZN**, respectively, compared to their room temperature peak emissions that can be attributed to the rigidochromic effect associated with the complexes having greater MLCT character of the emitting states. Even if both **FCZN** and **FZN** show similar room temperature emission peaks, the high dipole moment of **FCZN** could be the reason for more structural distortion in the excited state resulting in a higher difference of the room temperature and 77 K emission (25 nm, 1121 $cm^{-1}$) compared to a difference of 17 nm (752 $cm^{-1}$) in **FZN**. The 77 K emission attributes of **MeOFZN** show a less resolved vibrational progression, which could be due to the increase in the low-frequency vibrations (~400 $cm^{-1}$) associated with the change in metal–ligand bond length in the excited state compared to the high frequency ligand based vibrations.[6c] The **FCZN** and **FDZN** also show less resolution of the vibrational progressions than the parent **FZN** complex.

**Table 4** Excited state properties of the complexes[a]

| | FZN | FCZN | FDZN | MeOFZN |
|---|---|---|---|---|
| $E_{em}$(0–0)/$cm^{-1}$ | 467 | 460 | 456 | 452 |
| $\Delta\nu_{1/2}$/$cm^{-1}$ | 687 | 855 | 870 | 1122 |
| $\hbar\omega_M$/$cm^{-1}$ | 1293 | 1163 | 1268 | 892 |
| $S_M$ | 0.64 | 0.72 | 0.75 | 0.89 |

[a] $E_{em}$(0–0) was obtained from the peak emission wavelength in 2-methyltetrahydrofuran at 77 K. $\Delta\nu_{1/2}$ is the full width at half maximum for the (0–0) band and was obtained by the gaussian decomposition. $\hbar\omega_M$ was obtained from the energy difference of the first two emission peaks at 77 K. The Huang–Rhys factor, $S_M$ was estimated from the peak heights of the first two peaks of the emission spectra at 77 K.

The FWHM values of the resolved highest energy vibronic bands of **FZN**, **FCZN**, **FDZN**, and **MeOFZN** are 687, 855, 870 and 1122 $cm^{-1}$, respectively, implying again that the reorganizational energy of **MeOFZN** is highest in the excited state. The $\hbar\omega_M$ values of these complexes lie in the range of 892–1293 $cm^{-1}$ indicating that the dominant vibrational mode associated with the excited distortion can be ascribed to the aromatic in-plane and out-of-plane ring stretching and bending vibrations.[28–35] The

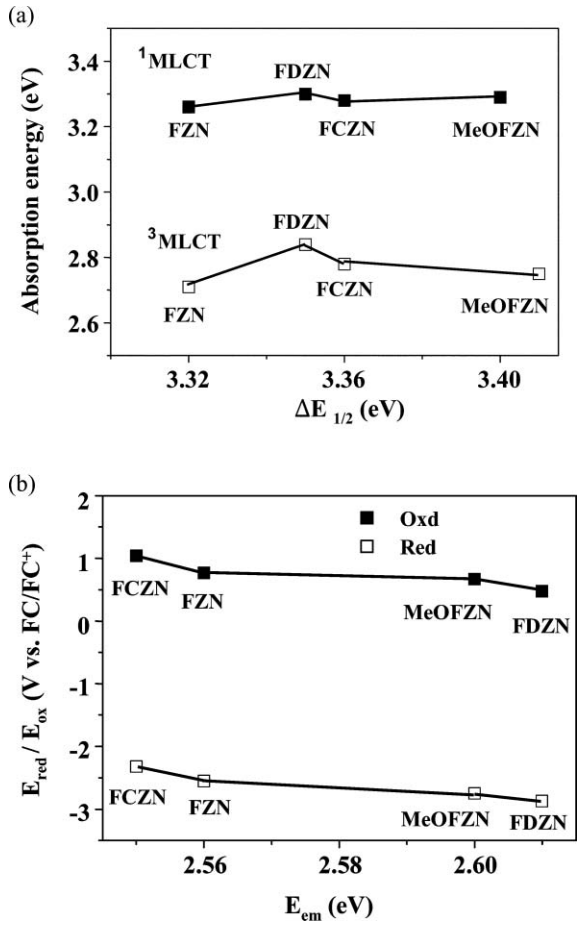


**Fig. 5** Comparative plot of (a) absorption energy *versus* $\Delta E_{1/2}$ and (b) $E$(red)/$E$(oxd) *versus* $\lambda_{em}$.

$S_M$ values (Huang–Rhys factors) of **FZN**, **FCZN**, **FDZN**, and **MeOFZN** are 0.64, 0.72, 0.75 and 0.89, respectively and are found to increase with the increase in the emission energies. The larger the $S_M$ value, the stronger the coupling between the dominant ligand-localized vibrations in the excited and ground states.[6c,36] The increase in the $S_M$ values with the increase in the emission energies is an indication of the decrease in the MLCT character of the excited state in the sequence of **FZN** > **FCZN** > **FDZN** > **MeOFZN** and more localization of the triplet state.[37]

The transient phosphorescence lifetimes ($\tau$) of the **FZN**, **FCZN**, **FDZN**, and **MeOFZN** complexes are 1.20, 1.50, 1.18 and 1.28 μs, respectively, as measured from 6% doped PMMA films. The photoluminescence (PL) quantum efficiencies of the complexes in the doped PMMA films are found to be 20, 40, 28 and 70% for **FZN**, **FCZN**, **FDZN**, and **MeOFZN**, respectively (Table 2). All the substituents enhance the quantum efficiency of the parent **FZN** complex. High quantum efficiencies of the cyclometalated Ir(III) complexes of 2-(4′,6-difluorophenyl)-4-methoxypyridine are reported by Chen *et al.*[38] The $k_r$ and the $k_{nr}$ values of the complexes follow the order of **MeOFZN** ($5.46 \times 10^5$ s$^{-1}$) > **FCZN** ($2.66 \times 10^5$ s$^{-1}$) > **FDZN** ($2.37 \times 10^5$ s$^{-1}$) > **FZN** ($1.75 \times 10^5$ s$^{-1}$) and **MeOFZN** ($2.34 \times 10^5$ s$^{-1}$) < **FCZN** ($4.00 \times 10^5$ s$^{-1}$) < **FZN** ($6.58 \times 10^5$ s$^{-1}$) < **FDZN** ($8.47 \times 10^5$ s$^{-1}$), respectively. Among the four complexes, only **MeOFZN** is found to have higher $K_r$ than $K_{nr}$. $K_r$ and $K_{nr}$ depend on the electronic nature of the transitions: $K_r$ through the electronic dipole moment integral and $K_{nr}$ through a vibrationally-induced electronic coupling integral. The $k_{nr}$ values of the complexes can be correlated to the nature of the substituents on the cyclometalating ligands.[6a,8] The pattern of the acceptor vibrations, which determine the non-radiative decay are different in the parent and substituted complexes. Among the substituted complexes, **FDZN** has the highest $k_{nr}$ values and lowest quantum efficiencies due to the distortional vibrations of the dimethyl amino group causing a great deal of nonradiative depopulation of the excited state.[8] However, we can presume that the methoxy substituent increases the coupling between the ground and excited states resulting in the increased $k_r$ values compared to the other complexes.

### Electrochemical and photophysical properties

The variations in the $^1$MLCT and $^3$MLCT absorption and peak emission energies of several Ir(III),[6] Os(II)[4] and Ru(II)[4] complexes exhibit similar patterns of acceptor parallel to the variations in $E_{1/2}$(oxd). A similar pattern of acceptor vibrations can not be expected in the present series of four compounds because of the electron-donating nature of the dimethylamino and methoxy groups and the electron-accepting nature of the cyano group, and their consequent effects on ring distortions, the electronic dipole moment, the vibrational parameters, and the σ- and π-donation of the cyclometalating ligands. Comparative plots of $^1$MLCT and $^3$MLCT absorption energies *versus* $\Delta E_{1/2}$ and $E$(red)/$E$(oxd) *versus* the peak emission energies are given in Fig. 5a and 5b, respectively. Little change in the $^1$MLCT and $^3$MLCT energies with the $\Delta E_{1/2}$ values is observed, contrary to the linear increase in the absorption and emission energies with $\Delta E_{1/2}$ of the previously reported Ir(III), Ru(II) and Os(II)[6d] complexes.

### Electroluminescence

Multilayer organic light emitting devices are fabricated by doping **FZN**, **FCZN**, and **FDZN** (5 wt%) in a blend of PS (polystyrene; used as a binder[39]) and mCP with the configuration of ITO/PEDOT-PSS (50 nm)/PS-mCP-dopant (20 : 74 : 6, 40 nm)/BAlq (40 nm)/LiF (0.9 nm)/Al (200 nm) (ITO = indium tin oxide, PEDOT-PSS = poly(3,4-ethylenedioxythiophene)–poly(styrenesulfonate)). The electroluminescence (EL) characteristics are summarized in Table 5. The EL spectra, external quantum efficiencies and I-V-L characteristics are demonstrated in Fig. 6 and 7, respectively. The shape of the EL spectra is different from the PL spectra in solution and film. The CIE coordinates are also shifted from the sky blue region to the greenish blue region. But in **FDZN**, the CIE coordinates are shifted to the more blue region. We attribute such spectral changes to the effect of the matrix on the excited state of the polar Ir(III) complexes.[8]

**Table 5** Electroluminescence properties

| | **FZN** | **FCZN** | **FDZN** |
|---|---|---|---|
| $\lambda_{EL}$/nm | 475, 501 | 465, 491 | 460 |
| ($x$, $y$) | (0.22, 0.41) | (0.20, 0.37) | (0.24, 0.32) |
| Turn-on $V$/V | 4.6 | 5.2 | 8.6 |
| Max. lum./cd m$^{-2}$ | 10 191 | 9905 | 1019 |
| Maximum $\eta_{ex}$ (%) | 2.4 | 3.7 | 1.2 |
| Maximum $\eta_L$/cd A$^{-1}$ | 5.5 | 7.8 | 2.3 |

 

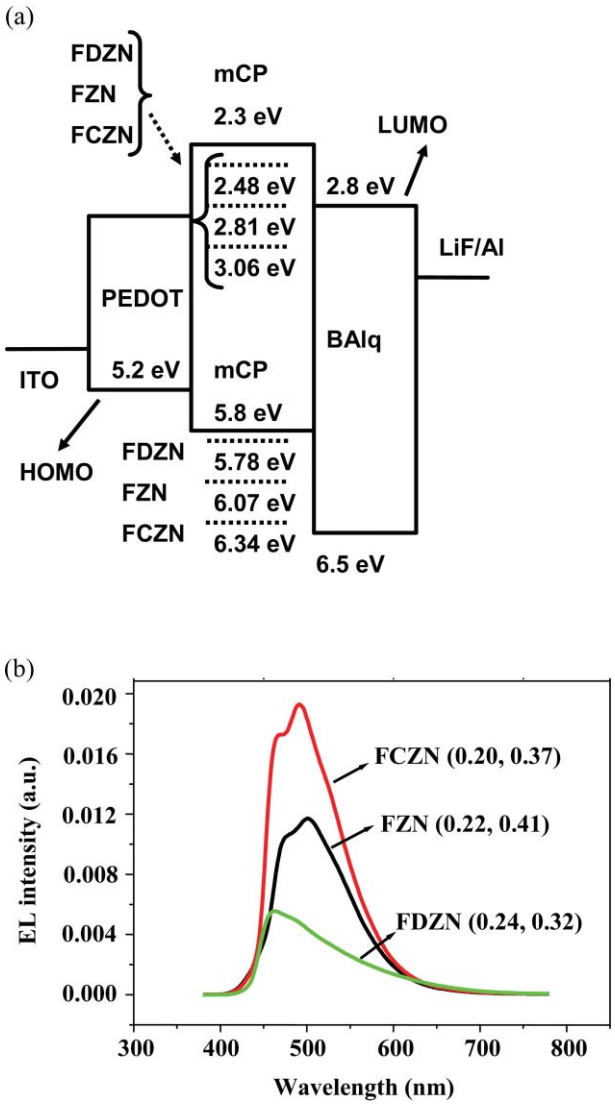


**Fig. 6** (a) Energy levels of the materials used in the device fabrication. (b) EL spectra obtained from the devices at 10 mA.

The device configuration and energy levels of the materials used in the device are shown in Fig. 6a. The HOMO levels of the Ir(III) complexes are determined from the SWV method. The LUMO and $^3$MLCT levels of the complex are calculated from the HOMO, $^1$MLCT optical absorption, and emission energies. The dopants have a deeper HOMO than that of the host except **FDZN** (5.78 eV), which is very close to the host HOMO (5.8 eV). This could allow the injection of the holes from mCP into the dopant **FDZN**, whereas it becomes increasingly difficult for hole injection from mCP to **FZN** (HOMO = 6.07 eV) and **FCZN** (HOMO = 6.34 eV). Again, a difference is observed in these three dopants as regards to the ease of electron injection from the host as well as the electron transporting material BAlq. The LUMO of **FDZN**, mCP and BAlq are 2.48, 2.3, and 2.8 eV respectively. Hence the electron injection from both mCP and BAlq to **FDZN** is easy. The LUMO of **FZN** (2.81 eV) is close to the LUMO of BAlq; hence electrons can be injected directly into **FZN** at the interface. But the electron transfer from mCP to **FZN** is not easy as there is a barrier of 0.5 eV. The electron transfer from mCP to **FCZN** is also difficult due to a gap of 0.8 eV, though electron transfer from BAlq is still possible. Thus **FDZN** is the most suitable dopant and should yield good device efficiency as the excitons from the host can be transferred into it along with the direct exciton formation on the dopant. At the other extreme, it is difficult to transfer the excitons from the host to the dopant **FCZN** due to energy level mismatch; rather excitons can be formed directly on **FCZN** due to electron trapping and the consequent recombination with a hole from the matrix. Moreover, **FCZN** possesses a high dipole moment of 9.68 D; this can lead to a local electric field, which can induce the charges, thus facilitating charge injection into the dopant. **FZN** offers an intermediate case where both the exciton formation on the dopant and transfer into the dopant from the host is possible.

As the result shows (Fig. 7) the **FCZN** device demonstrates a better performance than **FZN**, with a maximum external quantum efficiency ($\eta_{ex}$) of 3.7%, luminance efficiency ($\eta_L$) of 7.8 cd A$^{-1}$ at 0.08 mA cm$^{-2}$ and 8.8 V, a maximum brightness of 9916 cd m$^{-2}$ and 5.2 V turn-on voltage. The $\eta_{ex}$, $\eta_L$, maximum brightness and turn-on voltage of **FZN** are 2.4%, 5.5 cd A$^{-1}$ at 9.2 V and 0.12 mA cm$^{-2}$, 10 200 cd m$^{-2}$ and 5.6 V, respectively. Much lower $\eta_{ex}$ of 1.2% and $\eta_L$ of 2.3 cd A$^{-1}$ were observed for the **FDZN** device. The low EL efficiency of **FDZN** could arise due to the following reasons. From the energy level point of view it is likely that the holes stay on mCP, or at least go back and forth from the **FDZN** HOMO to the mCP HOMO, and exciton formation happens on mCP. 75% of the total mCP excitons are triplet excitons, which are transferred to **FDZN** in a delayed process or decay nonradiatively. Moreover, the distortional vibrations of the dimethylamino group causes a great deal of nonradiative depopulation of the excited state.[8] This is in agreement with the currently reported low efficiency of the device containing cyclometalated Ir(III) complexes of dimethylamino substituted 2,4-difluorophenyl pyridine ligand as the triplet emitter.[8] The higher PL quantum efficiency (40%) of **FCZN** and the direct exciton formation on **FCZN** as described in the previous paragraph could be the possible reason for the higher EL efficiency of the **FCZN**-based devices. The **FZN** device demonstrates higher current density than the **FCZN** device. This could be due to the charge trapping by **FCZN**. Since the triplet energies of the dopants (2.56 eV for **FZN**, 2.61 eV for **FDZN**, 2.55 eV for **FCZN**) are lower than that of the host (2.9 eV), the triplet exciton transfer from the host to the dopant is exothermic and can be considered as an efficient process. But a small difference of ~0.3 eV between the host and dopant triplet energies could lead to an endothermic backward triplet transfer from the dopant to the host.

## Conclusion

The different cyclometalating ligands alter the $^3$MLCT energies keeping the $^1$MLCT energy almost similar. The stabilization and destabilization of the HOMO and LUMO are specifically controlled by the electron accepting and donating substituents. The photoluminescence quantum efficiency and radiative emission rate are greatest and the nonradiative emission rate is lowest for **MeOFZN**. The complexes manifest rigidochromic effect with maximum reorganization energy in **MeOFZN**. $S_M$ value of **MeOFZN** also exhibits the dominance of the low frequency metal–ligand vibrations over the high frequency ligand-based vibrations.

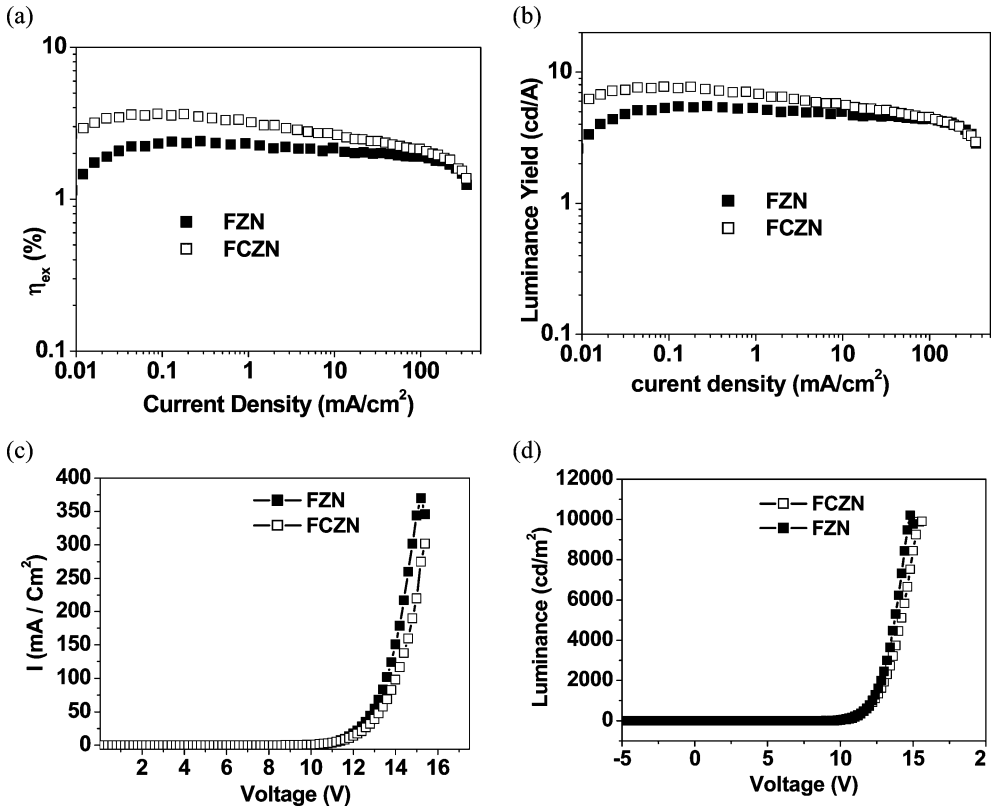


**Fig. 7** (a) External quantum efficiencies of the EL devices plotted against current density. (b) Luminous efficiencies of the EL devices plotted against current density. (c) Plot of current density *versus* voltage. (d) Brightness *versus* voltage.

The metal participation in the charge transfer state of **FDZN** is the highest among all the complexes. The substitutions increase the polar characteristics of the complexes, **FCZN** possessing the highest dipole moment among all the complexes. DFT results indicate the dominant participation of the pyrazole carboxamide ligand in the charge transfer process, particularly in **FCZN** and **FDZN**. The solution-synthesised OLED of **FCZN** doped in a blend of MCP and polystyrene showed an efficiency of 7.8 cd $A^{-1}$ with emission in the sky blue region.

## References


1 M. Maestri, V. Balzani, C. Deuschel-Cornioley and A. von Zelewsky, *Adv. Photochem.*, 1992, **17**, 1; N. Sutin, *Acc. Chem. Res.*, 1968, **1**, 225; T. J. Meyer, *Acc. Chem. Res.*, 1978, **11**, 94; B. Schmid, F. O. Garces and R. J. Watts, *Inorg. Chem.*, 1994, **32**, 9.

2 K. K.-W. Lo, C.-K. Chung, T. K.-M. Lee, L.-K. Lui, K. H.-K. Tsang and N. Zhu, *Inorg. Chem.*, 2003, **42**, 6886.

3 M. A. Baldo, S. Lamansky, P. E. Burrows, M. E. Thompson and S. R. Forrest, *Appl. Phys. Lett.*, 1999, **75**, 4; C. Adachi, M. A. Baldo, S. R. Forrest and M. E. Thompson, *Appl. Phys. Lett.*, 2000, **77**, 904; Y. Kawamura, S. Yanagida and S. R. Forrest, *J. Appl. Phys.*, 2002, **92**, 87; T. Tsutsui, M. J. Yang, M. Yahoro, K. Nakamura, T. Watanabe, T. Suji, Y. Fukuda, T. Wakimoto and S. Miyaguchi, *Jpn. J. Appl. Phys., Part 2*, 1999, **38**, L1502; C.-L. Li, Y.-J. Su, Y.-T. Tao, P.-T. Chou, C.-H. Chien, C.-C. Cheng and S.-R. Liu, *Adv. Funct. Mater.*, 2005, **15**, 387; X. Chen, J.-L. Liao, Y. Liang, M. O. Ahmed, H.-E. Tseng and S. A. Chen, *J. Am. Chem. Soc.*, 2003, **125**, 636; S.-J. Yeh, M.-F. Wu, C.-T. Chen, Y.-H. Song, Y. Chi, M.-H. Ho, S.-F. Hsu and C. H. Chen, *Adv. Mater.*, 2005, **17**, 285–289; S. Tokito, T. Lijima, Y. Suzuri, H. Kita, M. Suzuki and F. Sato, *Appl. Phys. Lett.*, 2003, **83**, 569–571; S. Tokito, M. Suzuki, F. Sato, M. Kamachi and K. Shrane, *Org. Electron.*, 2003, **4**, 105; C.-L. Lee, R. R. Das and J.-J. Kim, *Chem. Mater.*, 2004, **23**, 4642; C. Adachi, R. C. Kwong, P. Djurovic, V. Adamovich, M. A. Baldo, M. E. Thompson and S. R. Forrest, *Appl. Phys. Lett.*, 2001, **79**, 2082.

4 (*a*) S. R. Johnson, T. D. Westmoreland, J. V. Caspar, K. R. Barqawi and T. J. Meyer, *Inorg. Chem.*, 1988, **27**, 3195–3200; (*b*) E. M. Kober, J. L. Marshall, W. J. Dressick, B. P. Sullivan, J. V. Caspar and T. J. Meyer, *Inorg. Chem.*, 1985, **24**, 2755–2763; (*c*) J. V. Caspar and T. J. Meyer, *Inorg. Chem.*, 1983, **22**, 2444–2453.

5 M. G. Colombo, T. C. Brunold, T. Riedener, H. U. Gudel, M. Fortsch and H.-B. Burgi, *Inorg. Chem.*, 1994, **33**, 545–550; M. G. Colombo and H. U. Gudel, *Inorg. Chem.*, 1993, **32**, 3088; M. Maestri, D. Sandrini, V. Balzani, U. Maeder and A. von Zelewsky, *Inorg. Chem.*, 1987, **26**, 1323; A. B. P. Lever, *Inorganic Electronic Spectroscopy*, Elsevier, New York, 2nd edn, 1984, pp. 174–178.

6 (*a*) K. A. King, P. J. Spellane and R. J. Watts, *J. Am. Chem. Soc.*, 1985, **107**, 1431; (*b*) M. G. Colombo and H. U. Gudel, *Inorg. Chem.*, 1993, **32**, 3081; (*c*) R. J. Watts, *Comments Inorg. Chem.*, 1991, **11**, 303; (*d*) F. W. M. Vanhelmont, H. U. Gudel, M. Fortsch and H.-B. Burgi, *Inorg. Chem.*, 1997, **36**, 5512.

7 (*a*) K. Dedeian, P. I. Djurovich, F. O. Garces, G. Carlson and R. J. Watts, *Inorg. Chem.*, 1991, **30**, 1685; (*b*) S. Lamansky, P. Djurovich, D. Murphy, F. Abdel-Razzaq, Hae-Eun. Lee, C. Adachi, P. E. Burrows, S. R. Forrest and M. E. Thompson, *J. Am. Chem. Soc.*, 2001, **123**, 4304–4312; (*c*) J. Brooks, Y. Babayan, S. Lamansky, P. I. Djurovich, I. Tsyba, R. Bau and M. E. Thompson, *Inorg. Chem.*, 2002, **41**, 3055–3066; (*d*) J. Li, P. I. Djurovitch, B. D. Alleyene, M. Yousufudin, N. N. Ho, J. C. Thomas, J. C. Peters, R. Bau and M. E. Thompson, *Inorg. Chem.*, 2005, **44**, 1713–1727; (*e*) K. Dedeian, J. Shi, N. Shepherd, E. Forsythe and D. C. Morton, *Inorg. Chem.*, 2005, **44**, 4445; (*f*) P. Coppo, E. A. Plummer and L. De Cola, *Chem. Commun.*, 2004, 1774; (*g*) C.-H. Yang, S.-W. Li, Y. Chi, Y.-M. Cheng, Y.-S. Yeh, P.-T. Chou, G.-H. Lee, C.-H. Wang and C.-F. Shu, *Inorg. Chem.*, 2005, **44**, 7770; (*h*) T. Sajoto, P. I. Djurovich, A. Tamayo, M. Yousufuddin, R. Bau, M. E. Thompson, R. J. Holmes and S. R. Forrest, *Inorg. Chem.*, 2005, **44**, 7992; (*i*) F.-M. Hwang, H.-Y. Chen, P.-S. Chen, C.-S. Liu, Y. Chi, C.-F. Shu, F.-L. Wu, P.-T. Chou, S.-M. Peng and G.-H. Lee, *Inorg. Chem.*, 2005, **44**, 1344.

8 Y.-Y. Lyu, Y. Byun, O. Kwon, E. Han, W. S. Jeon, R. R. Das and K. Char, *J. Phys. Chem. B*, 2006, **110**, 10303.


 

9 (*a*) T.-H. Kwon, H. S. Cho, M. K. Kim, J.-W. Kim, J.-J. Kim, H. L. Kwan, S. J. Park, I.-S. Shin, H. Kim, D. M. Shin, Y. K. Chung and J.-I. Hong, *Organometallics*, 2005, **24**, 1578; (*b*) K. K. Lo, J. S. Chan, L. Lui and C. K. Chung, *Organometallics*, 2004, **23**, 3108.

10 R. J. Holmes, B. W. D. Andrade, S. R. Forrest, X. Ren and M. E. Thompson, *Appl. Phys. Lett.*, 2003, **83**, 3818; X. Ren, J. Li, R. J. Holmes, P. I. Djurovitch, S. R. Forrest and M. E. Thompson, *Chem. Mater.*, 2004, **16**, 4743.

11 P. J. Hay, *J. Phys. Chem. A*, 2002, **106**, 1634.

12 N. G. Park, G. C. Choi, J. E. Lee and Y. S. Kim, *Curr. Appl. Phys.*, 2005, **5**, 79.

13 S. Sprouse, K. A. King, P. J. Spellane and R. J. Watts, *J. Am. Chem. Soc.*, 1984, **106**, 6647.

14 W. Koch and M. C. Holthausen, *A Chemist's Guide to Density Functional Theory*, Wiley & Sons, New York, 2000; R. G. Parr and W. Yang, *Density Functional Theory of Atoms and Molecules*, Oxford University Press, Oxford, 1989; A. D. Becke, *J. Chem. Phys.*, 1993, **98**, 5648–5652; E. K. U. Gross and W. Kohn, *Adv. Quantum Chem.*, 1990, **21**, 255; R. Bauernschmitt and R. Ahlrichs, *Chem. Phys. Lett.*, 1998, **256**, 454; M. E. Casida, C. Jamorski, K. C. Casida and D. R. Salahub, *J. Chem. Phys.*, 1998, **108**, 4439; K. B. Wiberg, R. E. Stratmann and M. J. Frisch, *Chem. Phys. Lett.*, 1998, **297**, 60.

15 M. J. Frisch, G. W. Trucks, H. B. Schlegel, G. E. Scuseria, M. A. Robb, J. R. Cheeseman, V. G. Zakrzewski, J. A. Montgomery, Jr., R. E. Stratmann, J. C. Burant, S. Dapprich, J. M. Millam, A. D. Daniels, K. N. Kudin, M. C. Strain, O. Farkas, J. Tomasi, V. Barone, M. Cossi, R. Cammi, B. Mennucci, C. Pomelli, C. Adamo, S. Clifford, J. Ochterski, G. A. Petersson, P. Y. Ayala, Q. Cui, K. Morokuma, D. K. Malick, A. D. Rabuck, K. Raghavachari, J. B. Foresman, J. Cioslowski, J. V. Ortiz, A. G. Baboul, B. B. Stefanov, G. Liu, A. Liashenko, P. Piskorz, I. Komaromi, R. Gomperts, R. L. Martin, D. J. Fox, T. Keith, M. A. Al-Laham, C. Y. Peng, A. Nanayakkara, C. Gonzalez, M. Challacombe, P. M. W. Gill, B. G. Johnson, W. Chen, M. W. Wong, J. L. Andres, M. Head-Gordon, E. S. Replogle and J. A. Pople, *GAUSSIAN 98 (Revision A.9)*, Gaussian, Inc., Pittsburgh, PA, 1998.

16 S.-C. Chan, M. C. W. Chan, Y. Wang, C.-M. Che, K.-K. Cheung and N. Zhu, *Chem.–Eur. J.*, 2001, **7**, 4180; M. Kato, J. Takahasi, Y. Sugimoto, C. Kosuge, S. Kishi and S. Yano, *J. Chem. Soc., Dalton Trans.*, 2001, 747.

17 M. E. Thompson, R. Kwong, Y.-Z. Tung and J. Brooks, *US Pat.*, 0 025 993, 2005.

18 J. A. Turner, J. H. Christi, M. Vukovic and R. A. Osteryong, *Anal. Chem.*, 1977, **49**, 843.

19 R. S. Nicholson and I. Shain, *Anal. Chem.*, 1964, **36**, 706; J. Y. Kim, C. Lee and J. W. J. Park, *J. Electroanal. Chem.*, 2001, **504**, 104.

20 F. Neve and A. Crispini, *Eur. J. Inorg. Chem.*, 2000, 1039.

21 F. O. Garces, K. A. King and R. J. Watts, *Inorg. Chem.*, 1988, **27**, 3464.

22 Y. Ohsawa, S. Sprouse, K. A. King, M. K. DeArmond, K. W. Hanck and R. J. Watts, *J. Phys. Chem.*, 1987, **91**, 1047.

23 G. A. Carlson, P. I. Pjurovich and R. J. Watts, *Inorg. Chem.*, 1993, **32**, 4483.

24 E. M. Kober and T. J. Meyer, *Inorg. Chem.*, 1982, **21**, 3967.

25 J. N. Demas and G. A. Crosby, *J. Am. Chem. Soc.*, 1971, **93**, 2841; R. J. Watts, G. A. Crosby and J. L. Sansregret, *Inorg. Chem.*, 1972, **11**, 1474.

26 H. Yersin and D. Dongs, *Top. Curr. Chem.*, 2001, **214**, 81.

27 M. E. Thompson, P. I. Djurovich and R. Kwong, *WO Pat.*, 0 167 111, 2004.

28 N. Nakamato, *Infrared and Raman Spectra of Inorganic and Coordination Compounds*, Wiley, New York, 3rd edn, 1977.

29 E. M. Kober, J. V. Caspar, R. S. Lumpkin and T. J. Meyer, *J. Phys. Chem.*, 1986, **90**, 3722.

30 D. P. Rillema, C. B. Blanton, R. J. Shaver, D. C. Jackman, M. Boldaji, S. Bundy, L. A. Worl and T. J. Meyer, *Inorg. Chem.*, 1992, **31**, 1600.

31 G. H. Allen, R. P. White, D. P. Rillema and T. J. Meyer, *J. Am. Chem. Soc.*, 1984, **106**, 2613.

32 N. L. Damrauer, T. R. Boussie, M. Devenny and J. K. McCusker, *J. Am. Chem. Soc.*, 1997, **119**, 8253.

33 W. Humbs and H. Yersin, *Inorg. Chim. Acta*, 1997, **265**, 139.

34 H. Yersin, S. Schuetzenmeier, H. Wiedenhofer and A. von Zelewsky, *J. Phys. Chem.*, 1993, **97**, 13496.

35 H. Yersin, *Proc. SPIE–Int. Soc. Opt. Eng.*, 2004, **5214**, 124.

36 J. V. Caspar, T. D. Westmoreland, G. H. Allen, P. G. Bradley, T. J. Meyer and W. H. Woodruff, *J. Am. Chem. Soc.*, 1984, **106**, 3492.

37 H. Yersin, W. Humbs and J. Strasser, *Top. Curr. Chem.*, 1997, **191**, 153.

38 I. R. Laskar, S.-F. Hsu and T.-M. Chen, *Polyhedron*, 2005, **24**, 189.

39 H. Rudmann and M. F. Rubner, *J. Appl. Phys.*, 2001, **90**, 4338; H. Rudmann, S. Shimada and M. F. Rubner, *J. Am. Chem. Soc.*, 2002, **124**, 4918.